Metallurgical and Statistical Approaches to the Study of Cast Iron Street Furniture

C. SOFFRITTI, L. CALZOLARI, S. PEPI, A. FORTINI, M. MERLIN, and G.L. GARAGNANI

The evolution of microstructure in relation to dating and nationality of origin was investigated in twenty-four cast iron objects of street furniture produced between XIX and XX centuries in United Kingdom, France, and Italy. Chemical composition of the metalworks was evaluated by glow-discharge optical emission spectrometry. Fragments from the cast irons were analyzed by optical microscopy and scanning electron microscopy with energy-dispersive spectroscopy. Form, distribution, and size of graphite were evaluated in the microstructure according to standard EN ISO 945-1:2008. An image analysis software was employed to quantify the area fraction of graphite in the matrix, major axis, and shape factor of graphite lamellae, area fraction of manganese sulfides (ψ_S), area fraction of steadite, and number of eutectic cells per area unit. All data were grouped and linear discrimination analysis (LDA) was applied to assess the group assignment and the probability of correct classification for each metalwork. The results showed that the microstructural features were compatible with those of cast irons produced in the XIX and XX centuries. Values of ψ_S also suggested re-melting of cast irons, associated with recycling of cast iron and/or steel scraps. The high values of steadite found in the metalworks are probably due to the excellent castability required for complex shape castings in these centuries. The LDA multivariate analysis allowed to discriminate cast irons based on the year of manufacturing and the nationality of origin.

I. INTRODUCTION

THE prefect of the Seine Department of France from 1853 to 1870, George Eugène Haussman, first defined street furniture as "the whole series of objects or accessories which, installed in public and/or private spaces, provide functional services for the society." In those years, new elements were introduced in the modern cities to satisfy the requirements of safety, hygiene, comfort, and entertainment of the nascent bourgeoisie.[1,2] Street furniture included common objects in urban settlements such as street lamps, benches, balconies, grids, fountains, and gazebos; these elements were purposely created to improve the quality of life in the urban environments, evolving according to necessities along years and representing an essential part of the cities. The term "street furniture" also referred to the connection between the public space and private life, for example, a railing or a balustrade that delimited the private space of a balcony both reflected the taste of the house owner and acted as decor for the city in which they were placed.[1]

The massive diffusion in urban settlements of street furniture composed of cast iron alloys was connected to the First Industrial Revolution (1760 to 1840) and to the history of iron and steel industry. However, up to the second half of the XVIII century wrought iron was preferred for ornamental manufacturing, whereas cast iron was employed for structural components.[3] After the collapse of some cast iron structures, such as the Gray's Mill building in Manchester (United Kingdom), the trussed bridge over the river Dee, and the Wootton and Tay bridges, wrought iron was increasingly used for load-bearing applications. However, cast iron alloys continued to be employed for structural elements under compressive loads and non-structural applications including street furniture. The good castability and suitability to the production of numerous identical objects in a short time and on an industrial scale favored the use of cast iron alloys for street furniture. Nevertheless, wrought and cast iron continued to be used together, to complement the tensile capabilities of

C. SOFFRITTI, L. CALZOLARI, A. FORTINI, M. MERLIN, and G.L. GARAGNANI are with the Department of Engineering, University of Ferrara, Via Saragat 1, 44122 Ferrara, Italy Contact e-mail: chiara.soffritti@unife.it S. PEPI is with the Department of Physics and Earth Sciences, University of Ferrara, Via Saragat 1, 44121 Ferrara, Italy.

wrought iron and the compressive and decorative advantages of cast iron.[4]

Despite the constant presence in urban spaces of street furniture composed of cast iron alloys, its functional aspects have been almost always considered prevalent against artistic and historical values, therefore street furniture has been hardly associated with cultural heritage.[4] Accordingly, many historical objects for street furniture have been lost because they were considered obsolete and therefore replaced or re-melted.[5]

Few studies have been published about cast iron street furniture. Recently, the authors provided an overview of history of cast iron street furniture, focusing on the reasons behind the choice of cast iron alloys for street furniture in connection to the diffusion of cast iron during the First Industrial Revolution. The relationship between cast iron street furniture and cultural heritage was also analyzed, together with its development in the three main producing countries (United Kingdom, France, and Italy). The production technique and the importance of preservation of cultural heritage related to cast iron street furniture were also discussed.[6] In another study, the authors determined the state of conservation of three artifacts of historical cast iron street furniture by scanning electron microscopy with energy-dispersive spectroscopy (SEM/EDS), diffuse reflectance infrared Fourier transform (DRIFT) and μ-Raman spectroscopies, and electrochemical impedance spectroscopy (EIS).[7] In a previous study on this topic, the authors evaluated the protectiveness of ancient paints on historical street lamps made of cast iron alloys by X-ray diffractometry (XRD) and SEM/EDS, DRIFT, and EIS techniques.[8]

In this study, twenty-four cast iron metalworks of street furniture dating back to XIX and XX centuries were investigated to determine the evolution of microstructure in relation with dating and nationality of the foundry of origin. Twenty-one came from foundries located in United Kingdom, France, and Italy, and three whose origin was not reported. The chemical composition of the objects was evaluated by glow-discharge optical emission spectrometry. An extensive metallographic analysis was performed to quantify the parameters associated to graphite and matrix morphology and to other microstructural features of cast iron alloys. All data were grouped and the multivariate statistical technique linear discrimination analysis (LDA) was applied to assess the group assignment and to provide the probability of correct classification for each sample.

II. METALLURGICAL BACKGROUND OF THE STUDY

The term "cast iron alloys" identifies a large family of ferrous alloys with a carbon content greater than 2.0 pct.[9] The Chinese were the first people who intentionally used cast iron alloys during the Warring States period (475 to 221 B.C.) and more extensively in the Han Dynasty (206 B.C. to 220 A.D.). The earliest cast iron object is a lion produced in China and dating from 502 B.C. In pre-Roman and Roman periods of the European Iron Age (800 B.C. to 400 A.D.), the few objects made of cast iron alloys were imported from Far East; three examples are the fragments of a cauldron found in Nikolayevka (Ukraine) and dating around the IV to III century B.C., a fragment of a vessel found in the Roman Fort at Caerhun in North Wales (United Kingdom) and dating around 80 to 110 B.C., and the fragments of a cauldron found at Corby Glen (United Kingdom) and dating from the period following the Roman conquest of Britain in 43 B.C.[10]

The introduction of cast iron in Europe occurred around 1200 to 1450 A.D. Before this time, ironmaking was largely a rural and small-scale craft and most iron was produced by the bloomery process, involving the chemical reduction of red-hot wood charcoal, fluxes, and iron ores in a bloomery to obtain a spongy mass of metal intermixed with a semiliquid slag.[4] In the XIII century, the blast furnace technique was imported from China to produce cast iron alloys for military purposes, since wrought iron was not efficient to build weapons.[10] Blast furnace was larger and allowed higher wood charcoal/iron ores ratio than the bloomery. It was fed by air forced through water-powered bellows. The partially molten metal was run into sand molds at temperatures as high as 1450 °C, producing billets of cast iron, called "pigs." Before it could be used by the blacksmiths, the pigs were placed into a furnace called a "finery" to oxidize carbon and other impurities; the products were then forged into long rods.[6] Starting from the XVII century some resourceful British ironmasters attempted to improve the smelting procedure of cast iron alloys. In 1619, Jan Andries Moerbeck fueled the blast furnace by fluxes as limestone and iron ores (for example, hematite).[4] In 1709, Abraham Darby fueled the blast furnaces in Coalbrookdale by coke instead of wood charcoal, supporting larger charges of iron ores and limestone, and obtaining cast iron products with a lower percentage of sulfur.[11] Around 1720, the introduction in France of a new device, named cupola furnace, improved the process of the blast furnace. This device allowed secondary smelting to be poured on a large scale into complex castings for structural and decorative elements, such as columns, bridges, railings, and knockers.[4] In 1784, Henry Cort invented the reverberatory furnace in which iron ores were completed separated from fuel and the impurities removed from the molten metal by "puddling."[4] In 1776, John Wilkinson developed a steam-powered blower for blast furnaces, so that structural elements such as tie rods, angle irons, and tees could be produced on industrial scale. In 1863, United Kingdom became the largest producer of cast and wrought iron in Europe, followed by France.[4] At that time and until the end of the XIX century, Italy imported foreign workers and materials, limiting its cast iron production to duplicates of foreign designs.[1]

Historically, two main types of cast iron alloys were known, based on the appearance of their fracture surfaces: gray and white. The first one fractures along the graphite plates, with a matted and ductile fracture surface, whereas the second one fractures along the iron carbide (cementite), with a shiny and brittle fracture

surface.[9] White cast iron may also be softened by adding iron ores or hammer slags and exposing the mixture to high temperature for some days. Through this heat treatment, the brittle structure of this material is converted into the malleable form consisting of roughly spherical agglomerates of graphite in a ferritic or pearlitic matrix.[12] Although malleable iron was known since IV century B.C., this technique was first mentioned in an English patent dated 1670.[13] In 1896, the first paper discussing the physical properties of cast iron was published, including strength, deflection, hardness, grain, set, chill, and shrinkage. It also emphasized its low tensile strength in comparison to compression strength, due to the tendency to develop defects during the process of casting.[14] Between 1938 and 1949 Carl Adey, Henton Morrogh and Keith Millis invented ductile cast iron by adding magnesium and cerium: this type of cast iron exhibited a higher ductility in the as-cast form.[15] A lighter type of cast iron, compacted graphite iron, was patented in 1965.[16]

Concerning the chemical composition of cast iron alloys, the most common alloying elements are carbon, silicon, manganese, sulfur, and phosphorous. The amount of carbon varies significantly depending on the grade of pig iron and scraps used, but generally it ranges from 2.0 to 4.3 pct.[9] When a percentage of silicon between 0.5 and 3.0 pct is added, the formation of graphite instead of cementite is promoted during solidification.[17] When the percentage of silicon is over 3.0 pct, strength, hardness, hardenability, wear, and corrosion resistance of cast iron alloys are increased.[9] Manganese is added to neutralize the effects of sulfur, a detrimental element when present, since sulfur forms a low-melting phase (iron sulfide, FeS) and prevents the nucleation of graphite. It is universally accepted that the manganese concentration should be in excess of the stoichiometric ratio (Mn:S = 1.7:1) to favor the formation of manganese sulfide (MnS) instead of iron sulfide.[18] Some authors also suggested a Mn:S ratio 2:7.[19] Concerning phosphorous, its solubility in austenite decreases with increasing carbon percentage, thus phosphorous segregates into the melt during solidification of cast iron.[20] For casting in sand molds and in the absence of carbide-forming elements such as chromium and vanadium, phosphorous forms a eutectic phosphide (steadite). Steadite is a eutectic of ferrite and iron phosphide (Fe_3P), containing 10.2 pct phosphorous and 89.8 pct iron.[21] When the percentage of phosphorous is lower than 0.005 pct, steadite particles become visible at room temperature in areas where solidification occurs last, whereas when this element is higher than 0.2 pct separate particles of steadite solidify as concave triangular constituents.[22] Finally, when the percentage of phosphorous is higher than 0.4 pct, cellular networks of steadite surround eutectic cells and dendrites.[23]

III. MATERIALS AND METHODS

Twenty-four cast iron artifacts of street furniture dating back to the XIX and XX centuries were conferred to Department of Engineering of the University of Ferrara (Ferrara, Italy) by the Neri Foundation – The Italian Museum of Cast Iron (Longiano, Forlì-Cesena, Italy). Twenty-one artifacts came from foundries located in United Kingdom, France, and Italy, and three were of unreported origin. The cast iron objects were parts of street lamps replaced by identical copies during restoration, and two of them were part of a greenhouse and a bench, respectively. For comparison, five artifacts belonging to modern street lamps in cast iron were also investigated. A summary of the analyzed cast iron parts is reported in Table I, together with information on identification number, year of manufacturing, nationality of the foundry of origin, and a short description of the street furniture from which they were collected.

The chemical composition of CI parts was evaluated by glow-discharge optical emission spectrometry (GDOES). The instrument was a SPECTRUMA GDA 650 (SPECTRO Analytical Instruments, Kleve, Germany) spectrometer with a Grimm-style glow-discharge lamp in direct current mode. Discharge conditions were 700 V voltage, 20 mA current, and sputtering time of 150 s. The internal diameter of the tubular anode (hence the analyzed area in each measurement) was 2.5 mm. The Grimm-type atomization/excitation source was evacuated by a rotary pump to a final pressure of 0.05 hPa. After evacuation, flowing argon as a working gas (99.995 pct purity) was introduced to a constant pressure of 3.35 hPa.

The microstructural characterization was performed on representative fragments obtained from the cross-section (sample observed across the thickness of the metal). The fragments were embedded in mounting resin, polished and analyzed by a Leica MEF4M optical microscope (Leica, Wetzlar, Germany) to determine form, distribution, and size of graphite, in accordance with the standard EN ISO 945-1:2008.[24] The microstructure was analyzed after chemical etching with Nital 4 (4 pct nitric acid HNO_3 in ethanol) by the same optical microscope and by a Zeiss EVO MA 15 (Zeiss, Oberkochen, Germany) scanning electron microscope (SEM), equipped with an Oxford X-Max 50 (Oxford Instruments, Abingdon-on-Thames, United Kingdom) energy-dispersive microprobe for semi-quantitative analyses (EDS).

The micrographs of the center parts of cross-sections were processed by Leica Application Suite (LAS, Leica) image analysis software to quantify the following microstructural features: area fraction of graphite (ψ_G) in the matrix, major axis of graphite lamellae (MA) (i.e., the lamellae length), shape factor of graphite lamellae (SF), area fraction of manganese sulfides (ψ_S), area fraction of steadite (EP), and number of eutectic cells per area unit (EC). The evaluation of area fraction of graphite, major axis, and shape factor of graphite lamellae was conducted on five unetched micrographs per microstructure, with about 400 to 600 lamellae per micrograph (area: 0.33 x 0.45 mm^2). To determine ψ_G, the area of the single graphite lamella in each micrograph was calculated by the LAS software; these areas were added up and divided by the field area of the micrograph to obtain the area fraction of graphite in the

matrix. Five values of ψ_G per microstructure were quantified. Concerning the major axis of graphite lamellae, this parameter is defined as the greatest distance (measured by the LAS software) between parallel lines drawn through two points at the edges of the graphite lamellae, regardless of orientation. This distance is also called maximum feret (F_{max}). The shape of graphite lamellae was expressed in the form of a numeric value through the shape factor, defined as SF $= (16A^2)/(\pi PF_{max}^3)$, where A is the surface area and P is the perimeter of the graphite lamella (calculated by the LAS software). The shape factor ranges from 0 for a line to 1 for a perfect circle.[25,26] About 400 to 600 values of MA and SF per micrograph were quantified, for a total of five micrographs per microstructure.

The area fraction of manganese sulfides was determined on ten unetched micrographs per microstructure, with about 5 to 8 particles per micrograph (area: 0.13 x 0.18 mm^2). The area fraction of steadite was evaluated according to a previously published method,[20] after color etching with Murakami reagent (10 g potassium ferricyanide $K_3Fe(CN)_6$, 10 g potassium hydroxide KOH, 75 ml distilled water). The typical microstructure revealed by color etching using Murakami reagent is shown in Figure 1(a), in which a light-brown cellular network of steadite is visible, surrounding dendrites. A total of fifteen micrographs (area of each micrograph: 0.33 x 0.45 mm^2) were analyzed for each fragment. Measurements of the area fractions of manganese sulfides and steadite were conducted following the same procedure used for the area fraction of graphite in the matrix (calculated by the LAS software), thus fifteen values of ψ_S and EP per microstructure were quantified.

The number of eutectic cells per area unit is an index of the nucleation susceptibility of graphite.[9] It was determined after color etching with sodium picrate reagent (2 g picric acid $C_6H_3N_3O_7$, 25 g sodium hydroxide NaOH, 100 ml water[27]). When exposed to the polarized light of the optical microscope after color etching using sodium picrate reagent, the eutectic cell boundaries exhibited an approximately circular shape and a blue appearance as a result of entrapment of impurities, such as phosphorous and sulfur, at the interface (Figure 1(b)). Measurements of the number of eutectic cells per area unit were carried out at low magnification ($\times 5$) in accordance to a previously published method.[28] Based on this method, the number of eutectic cells per area unit is defined as EC $= (N_i + 0.5N_w + 1)/F$, where N_i is the number of eutectic cells inside the rectangle S, N_w is the number of eutectic cells that intersect the sides of S, but not their corners, and F is the surface area of S. A total of fifteen images (area of each image: 6.33 x 3.35 mm^2) were analyzed for each fragment. Six micrographs were merged to generate each image processed by the image analysis software. Fifteen values of EC per microstructure were quantified.

All data were grouped according to two classifications, the first one based on dating (second half XIX century, early XX century, and XXI century) and the second one on the nationality of the foundry of origin (United Kingdom, France, Italy, and unreported). To verify the differences among group means in all data, the Kruskal–Wallis non-parametric test (with *post hoc* Dunn's test) was employed. Linear discriminant analysis (LDA) was chosen as the most appropriate multivariate statistical technique for the interpretation of all data. In LDA, the user must assign group classifications to the data sets and the differences among these predetermined groups describe combinations of variables.[29] Stepwise LDA was applied to variables by a Wilk's Lambda test (*p* value < 0.01) and an F-statistic factor.[29] The variables were tested by cross validation randomly choosing 3 samples out of 31 as outgroup and applying discriminant analysis. This analysis assesses the group assignment and uses the generated discriminant model to reclassify the data, providing the probability of correct classification for each sample. The high percentage of cross validation in our samples supported a successful discrimination among groups. All data analyses were carried out by means of the software XLSTAT (Version 2015.5.02, Addinsoft, Paris, France).

IV. RESULTS AND DISCUSSION

The chemical composition of alloys (measured by GDOES) in the examined CI parts is reported in Table II.

Based on the results, the artifacts consisted of Fe-C alloys in which the amount of carbon ranged from 2.9 to 3.6 pct; accordingly, they could be considered as hypoeutectic cast irons. In all metalworks, the percentage of silicon was between 1.6 and 3.0 pct. As previously mentioned, its addition in these concentrations was able to promote the nucleation of graphite during solidification.[17] The minimum and maximum contents of manganese were 0.3 and 1.1 pct, respectively, whereas the amount of sulfur ranged from 0.04 to 0.18 pct. For the cast iron alloys dating to the second half of XIX century and for those dating to the early XX century, the percentage of phosphorous was between 0.42 and 1.12 pct. All phosphorous values were also higher than 0.4 pct, which was indicated in Section II. as the lower limit for the formation of cellular networks of steadite surrounding eutectic cells and dendrites. Conversely, metalworks dating to the early XXI century showed very low concentrations of this element (from 0.03 to 0.22 pct).

According to the standard EN ISO 945-1:2008, all cast irons could be classified as gray cast irons. Lamellar (flake) graphite with sharp ends (graphite form I) was observed in all fragments with the exception of CI_1, in which also aggregates of graphite flakes (graphite form II) were detected. Among cast irons, 52 pct were composed of lamellar graphite of Type B (rosette grouping with random orientation), 24 pct of lamellar graphite of Type C (aggregate of larger graphite flakes surrounded by smaller, randomly oriented graphite flakes), 14 pct of lamellar graphite of Type A (apparently uniform distribution), and 10 pct of lamellar graphite of Type D (fine, randomly oriented graphite flakes in the interdendritic position) (Figure 2(a)). It should be pointed out that in the cast irons CI_8, CI_8_1, CI_12, CI_14, CI_18, and CI_28 the lamellar

Table I. Summary of Analyzed Cast Iron (CI) Parts, Reporting Their Identification Number, the Year/Years of Manufacturing, the Nationality of the Foundry of Origin, and a Short Description of the Street Furniture from which they Were Collected

Identification Number	Year/Years of Manufacturing	Nationality	Description
CI_1	1846	Italy	window of greenhouse
CI_2	1870	France	column of street lamp
CI_3	1870 to 1880	Italy	base of street lamp
CI_4	1850 to 1900	n.r.	column of street lamp
CI_5	1880	Italy	column of street lamp
CI_6		Italy	column of street lamp
CI_7	1880 to 1890	Italy	column of street lamp
CI_8*		United Kingdom	base of street lamp
CI_8_1*		United Kingdom	base of street lamp
CI_9		Italy	column of street lamp
CI_10	1890	Italy	base of street lamp
CI_11		Italy	top of street lamp
CI_12		Italy	base of street lamp
CI_13	1890 to 1900	Italy	column of street lamp
CI_14		Italy	column of street lamp
CI_15	1896	Italy	bracket of street lamp
CI_16	1900	n.r.	bracket of street lamp
CI_17		Italy	base of street lamp
CI_18	1910	France	decoration of street lamp
CI_19		Italy	base of street lamp
CI_20**		United Kingdom	base of street lamp
CI_20_1**		United Kingdom	base of street lamp
CI_21	1910 to 1920	Italy	base of street lamp
CI_22	1920	n.r.	leg of bench
CI_23	1929	Italy	top of street lamp
CI_24	1930	France	base of street lamp
CI_25	2019	Italy	decoration of street lamp
CI_26		Italy	decoration of street lamp
CI_27		Italy	decoration of street lamp
CI_28		Italy	column of street lamp
CI_29		Italy	column of street lamp

n.r. = not reported.
*The objects named CI_8 and CI_8_1 were part of the same street lamp.
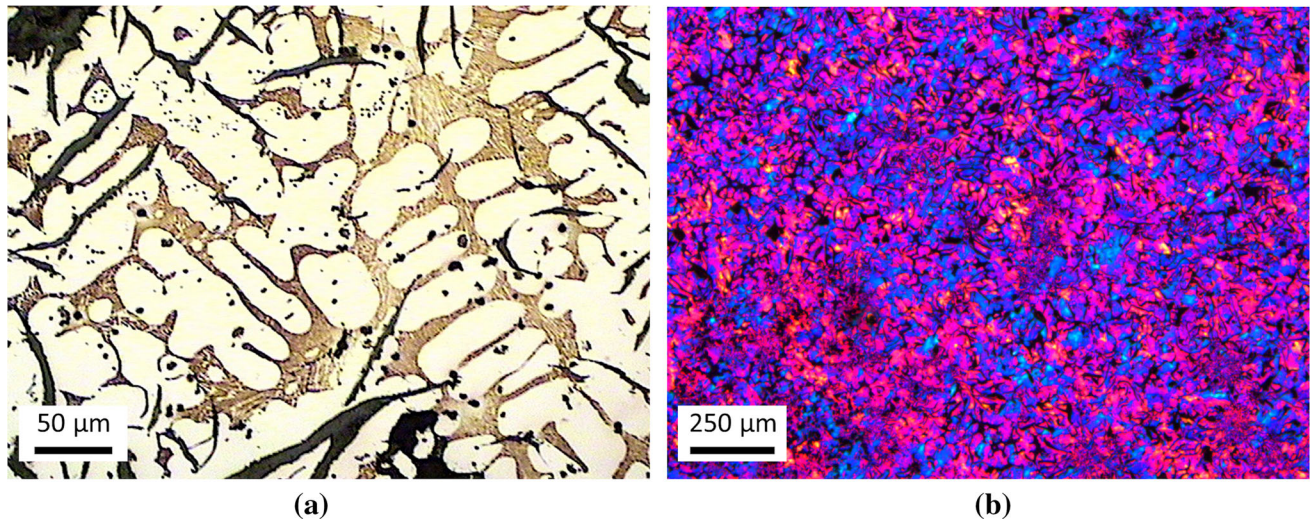**The objects named CI_20 and CI_20_1 were part of the same street lamp.

Fig. 1—Optical micrographs showing the typical microstructures revealed by color etching with (*a*) Murakami and (*b*) sodium picrate reagents.

graphite of Type B was detected in association with a percentage of the lamellar graphite of Type D lower than 10 pct. Concerning the size of graphite lamellae, 3 pct of cast irons contained lamellae lengths between 0.50 and less than 1.00 mm (size 2), 15 pct between 0.25 and less than 0.50 mm (size 3), 42 pct between 0.12 and

less than 0.25 mm (size 4), 34 pct between 0.06 and less than 0.12 mm (size 5), 3 pct between 0.03 and less than 0.06 mm (size 6), and 3 pct less than 0.015 mm (size 8) (Figure 2(b)). It is known that form, distribution, and size of graphite depend on cooling rates, degree of undercooling, cast impurities and additives, inoculation, and overheating of the molten liquid.[9] For the cast iron samples examined, no data were available about their

Table II. Chemical Composition of Alloys (Measured by GDOES, Weight pct) in the Examined CI Parts

CI Part	C	Si	Mn	P	S	Fe	Others
CI_1	3.5	2.0	1.1	0.82	0.04	91.7	balance
CI_2	3.1	2.7	0.3	1.01	0.07	91.6	balance
CI_3	3.6	1.8	0.8	1.01	0.08	92.2	balance
CI_4	3.1	1.8	0.3	0.82	0.04	93.3	balance
CI_5	3.3	3.0	0.7	0.93	0.15	91.2	balance
CI_6	3.3	2.3	1.0	0.79	0.10	92.1	balance
CI_7	3.1	1.9	0.8	0.90	0.05	92.8	balance
CI_8	3.2	1.8	0.7	1.00	0.07	92.5	balance
CI_8_1	3.2	1.8	0.7	0.98	0.08	92.6	balance
CI_9	3.3	2.4	1.0	0.81	0.12	91.9	balance
CI_10	3.3	2.5	1.0	0.86	0.09	91.7	balance
CI_11	3.5	2.5	1.4	0.92	0.05	90.9	balance
CI_12	2.9	3.0	0.5	0.77	0.08	91.2	balance
CI_13	3.1	2.4	1.0	0.97	0.12	92.0	balance
CI_14	3.2	2.2	1.0	0.94	0.08	92.0	balance
CI_15	3.4	3.0	0.9	0.63	0.04	91.4	balance
CI_16	3.3	1.6	0.4	0.74	0.18	93.2	balance
CI_17	3.1	1.9	0.4	1.12	0.09	92.5	balance
CI_18	3.4	1.6	0.3	0.79	0.14	93.2	balance
CI_19	3.1	2.2	0.4	1.00	0.10	92.6	balance
CI_20	3.4	2.1	0.6	0.68	0.12	92.5	balance
CI_20_1	3.3	2.1	0.6	0.67	0.11	92.6	balance
CI_21	3.2	2.4	0.5	1.10	0.11	91.9	balance
CI_22	3.3	2.0	0.4	0.78	0.15	92.7	balance
CI_23	3.3	1.6	0.4	0.88	0.12	93.0	balance
CI_24	3.2	2.1	0.7	0.42	0.11	91.0	balance
CI_25	3.4	2.5	0.5	0.03	0.07	93.0	balance
CI_26	3.5	2.0	0.6	0.18	0.12	93.1	balance
CI_27	3.4	1.9	0.6	0.20	0.12	93.2	balance
CI_28	3.5	2.3	0.6	0.22	0.11	92.6	balance
CI_29	3.2	2.1	0.4	0.03	0.09	93.2	balance

Each Artifact was Measured in Triplicate.

manufacturing techniques. However, the lamellar graphite of Type B is typical of alloys solidified with intermediate degrees of undercooling, except when it is associated with a lamellar graphite of Type D: a mixed distribution of lamellar graphite is typical of castings solidified with higher degrees of undercooling.[9,24] The lamellar graphite of Type C appears frequently in thin-walled castings, whereas the lamellar graphite of Type A suggests a low-to-intermediate degree of undercooling and a sufficient inoculation treatment.[9] Examples of graphite lamellae distributions of Type A-D observed in cross-sections of the analyzed fragments are shown in Figures 3(a) through (d).

Microstructures observed in the cross-sections of the cast irons after chemical etching with Nital 4 were mainly pearlitic with ferrite close to the graphite lamellae, steadite, and impurities in the form of polygonal shape particles (Figures 4(a) through (c)). These particles were identified as manganese sulfide inclusions by semi-quantitative SEM/EDS analyses. Unlike steels, where manganese sulfide inclusions are intentionally obtained to improve machinability, cast irons show these inclusions as a natural result of the foundry process.[9] The steadite observed on the analyzed artifacts was in the form of cellular networks surrounding dendrites, also in those with a percentage of phosphorous lower than 0.4 pct. The addition of phosphorous lowers the melting point and improves the fluidity of cast irons, allowing to create nearly unlimited decorative and structural components with thin wall thickness.[2,4,8] There were no detectable differences between the microstructures observed in cross-sections close to the surface and in the center of the cast irons. Therefore, the cast iron samples examined were very uniform in appearance and could be repetitively produced.

Tables III and IV show the values of microstructural features determined by image analysis of the micrographs in cross-section of the cast irons and grouped according to dating and nationality of the foundry of origin. Statistically significant differences for dating (p value < 0.05) were obtained for MA, ψ_S, and EP (Table III), but for the nationality of the foundry of origin statistically significant differences were found for ψ_G, ψ_S, and EC (Table IV).
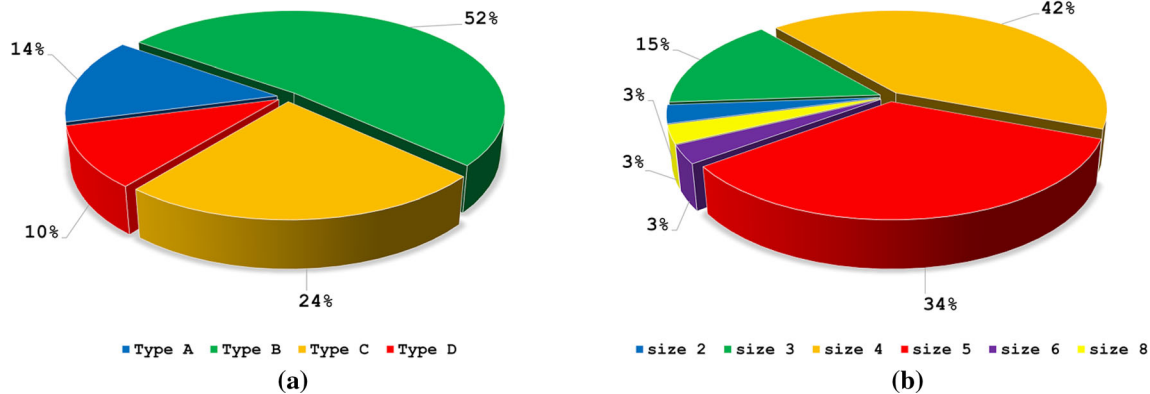

Fig. 2—Pie charts of (a) distribution and (b) size of graphite lamellae in cross-sections of the analyzed cast irons.
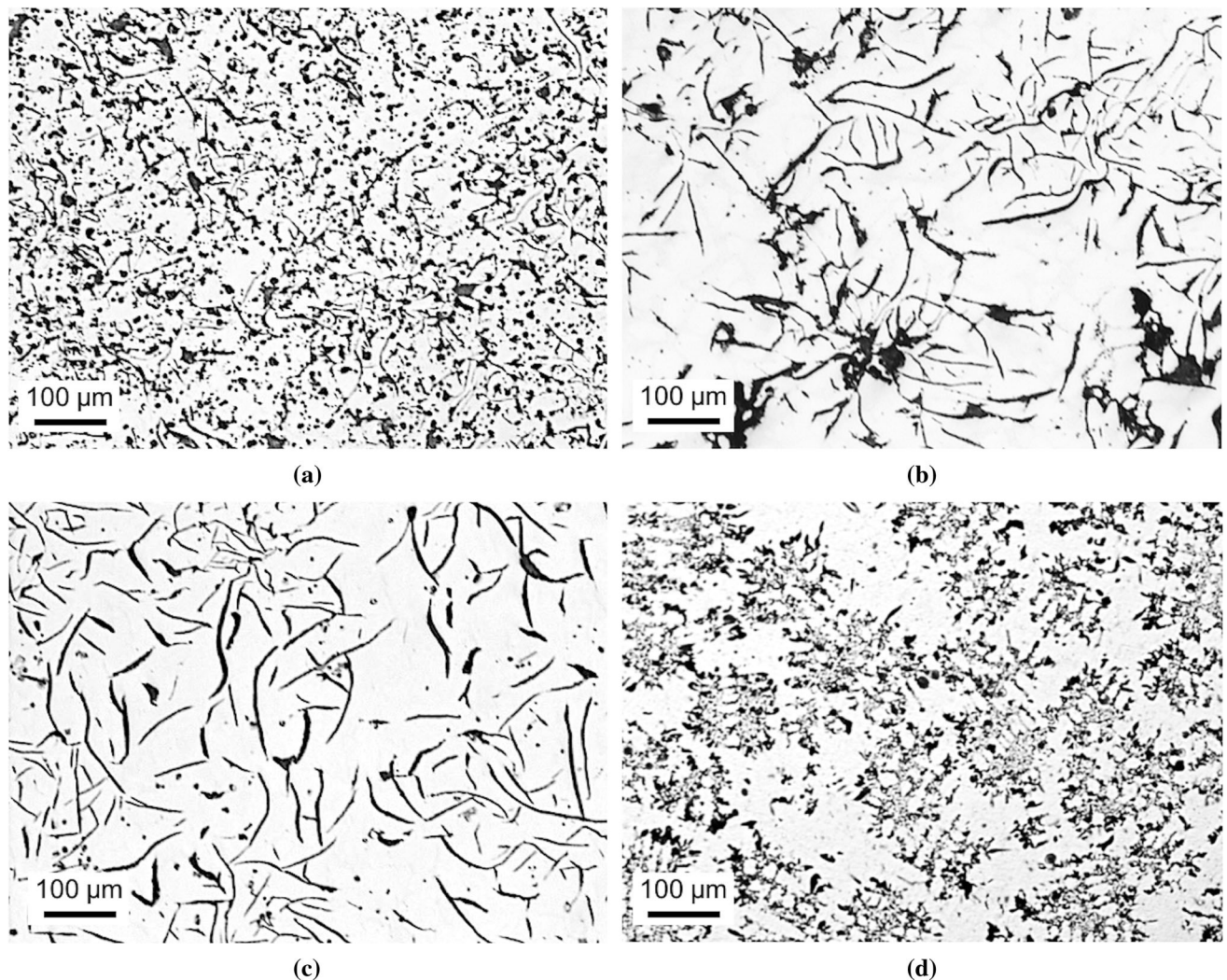
Fig. 3—Optical micrographs of the unetched microstructures observed in cross-sections of the analyzed cast irons: (*a*) graphite lamellae distribution of Type A in CI_1; (*b*) graphite lamellae distribution of Type B in CI_7; (*c*) graphite lamellae distribution of Type C in CI_6; (*d*) graphite lamellae distribution of Type D in CI_24.

Box plots of area fraction of graphite in the matrix determined by image analysis of the optical micrographs in cross-section of the cast irons are shown in Figure 5. Considering the artifacts dating to the second half of XIX century (box plots referring to cast iron samples from 1 to 15), the median value of the area fraction of graphite was the highest in CI_4 (ψ_G = 25 pct), and the lowest in CI_5 (ψ_G = 10 pct). Among the cast iron samples dating to the early XX century (box plots referring to samples from 16 to 24), the highest value was detected in CI_20 (ψ_G = 20 pct) and the lowest in CI_17 (ψ_G = 13 pct). Among the cast iron samples dating to the early XXI century (box plots referring to samples from 25 to 29), the highest value was detected in CI_25 (ψ_G = 18 pct) and the lowest in CI_29 (ψ_G = 11 pct). Considering all cast iron samples, the maximum and minimum values were those of CI_4 and CI_5. The amount of graphite and size, morphology, and distribution of graphite lamellae depend on chemical composition before the casting process, on inoculants and cooling conditions.[30,31] The four oldest cast irons

(CI_1, CI_2, CI_3, CI_4) showed higher ψ_G due to low cooling rates and low-to-intermediate degrees of undercooling, proved by the prevalence of lamellar graphite of Type A in these artifacts. From late XIX century onwards, the area fraction of graphite decreased with increasing cooling rate and the lamellar graphite of Type B (intermediate degrees of undercooling) replaced the lamellar graphite of Type A in all cast irons except CI_8, CI_12, CI_14, CI_20, and CI_25. These last artifacts mainly showed lamellar graphite of Type B + D and C.

Box plots of major axis of graphite lamellae determined by image analysis of the optical micrographs in cross-section of the cast irons are shown in Figure 6. Considering the artifacts dating back to the second half of XIX century (box plots referring to cast iron samples from 1 to 15), the median value of the major axis of graphite lamellae was the highest in CI_10 (MA = 35 μm), and the lowest in CI_14 (MA = 18 μm). Among the cast iron samples dating to the early XX century (box plots referring to samples from 16 to 24), the
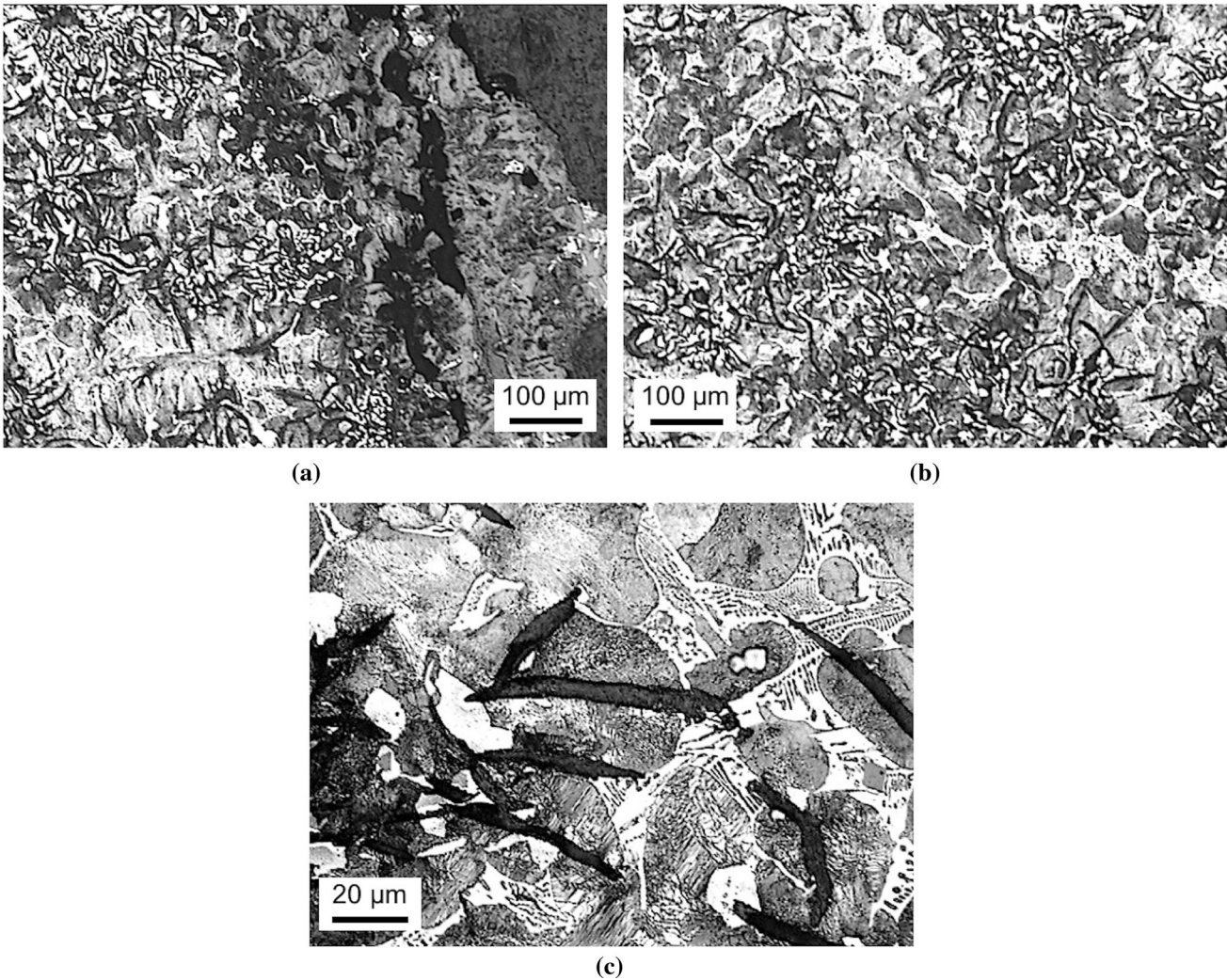
(a)

(b)

(c)

Fig. 4—Optical micrographs of the microstructure observed in cross-section of CI_11, after chemical etching with Nital 4: (*a*) overview of microstructure close to the surface; (*b*) overview of microstructure in the center; (*c*) details of cellular network of steadite surrounding dendrites.

highest value was detected in CI_16 (MA = 37 μm) and the lowest in CI_17 (MA = 21 μm). Among the cast iron samples dating to the early XXI century (box plots referring to samples from 25 to 29), the highest value was detected in CI_26 (MA = 21 μm) and the lowest in CI_25 (MA = 15 μm). Considering all cast iron samples, the maximum and minimum values were those of CI_16 and CI_25. For all metalworks, in the same cast iron sample the major axis of graphite lamellae was strongly variable, as proved by the large number of outliers: for example, in CI_3 the lamellae length ranged from 0.0066 to 0.25 mm and in CI_20 from 0.0057 to 0.26 mm. According to the standard EN ISO 945-1:2008, the size of graphite is determined through comparison with reference images. As established by the standard, the comparison of micrographs with these images depends on the subjective impression of the metallographer. Sizes are indicated by a progressive number from 1 to 8, with a maximum size of the lamellae ranging from ≥ 1 mm (size 1) to < 0.015 mm (size 8). The box plots in Figure 6 prove that this classification is overly simplified in comparison with

measurements of the major axis of graphite lamellae by image analysis, which represent a better estimate of the size of graphite in all artifacts. In agreement with previous studies,[30,32] even when the morphology of graphite is apparently similar, there are differences in the length of graphite lamellae that could be due to variable thickness of the castings.

Box plots of shape factor of graphite lamellae determined by image analysis of the optical micrographs in cross-section of the cast irons are shown in Figure 7. In all cases, the median SF values were lower than 0.1 (the maximum value detected for CI_13), as confirmed by the presence of elongated graphite lamellae with sharp ends in all metalworks (graphite form I, in accordance with the standard EN ISO 945-1:2008). Although none of the differences in SF values was statistically significant, the large number of outliers suggested the occurrence of less elongated and more curved graphite lamellae.
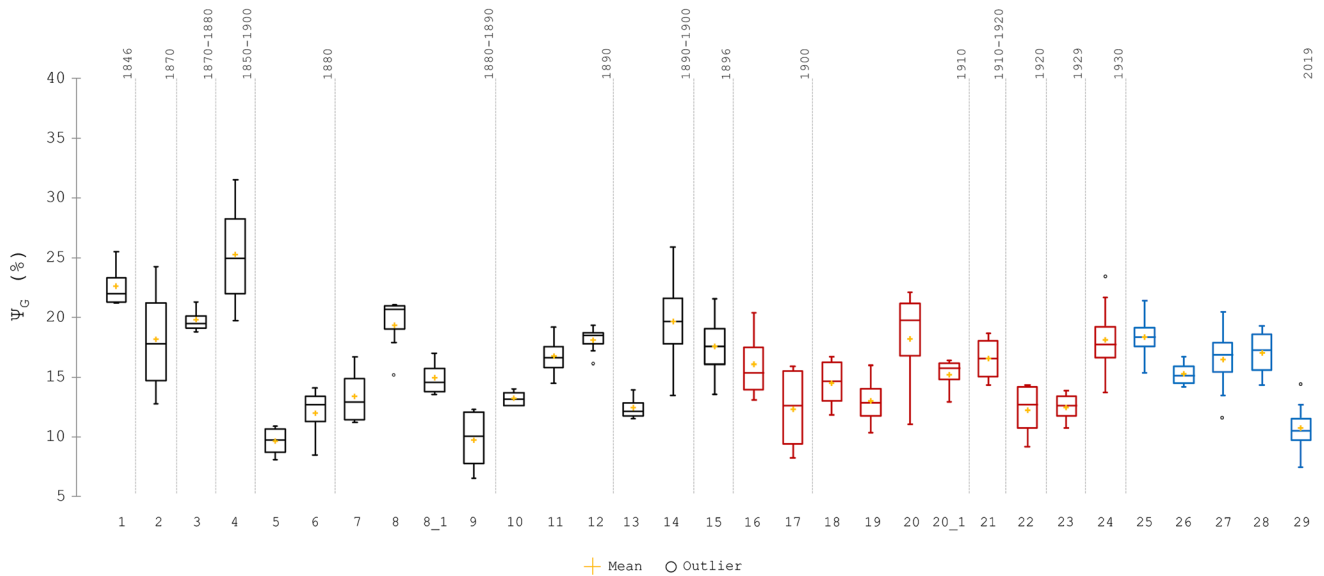
Box plots of area fraction of manganese sulfides determined by image analysis of the optical micrographs in cross-section of the cast irons are shown in Figure 8.

Table III. Values of Microstructural Features Determined by Image Analysis of the Micrographs in Cross-Section of the Cast Irons, Grouped According to Dating and Analyzed by Kruskal–Wallis Non-parametric Test with *Post Hoc* Dunn's Test

Microstructural Features	Second Half XIX Century	Early XX Century Median	Early XXI Century	p value
ψ_G (Pct)	17	14	17	n.s.
MA (μm)	31	31	21	**
SF	0.07	0.06	0.07	n.s.
ψ_S (Pct)	0.3	0.5	0.5	**
EP (Pct)	10	12	1	***
EC (cm^{-2})	17	18	21	n.s.

ψ_G, area fraction of graphite in the matrix; MA, major axis of graphite lamellae; SF, shape factor of graphite lamellae; ψ_S, area fraction of manganese sulfides; EP, area fraction of steadite; EC, number of eutectic cells per area unit.
p values: ** < 0.01; *** < 0.001; n.s. = not significant.

Table IV. Values of Microstructural Features Determined by Image Analysis of the Micrographs in Cross-Section of the Cast Irons, Grouped According to Nationality of the Foundry of Origin and Analyzed by Kruskal–Wallis Non-parametric Test with *Post Hoc* Dunn's Test

Microstructural Features	United Kingdom	France Median	Italy	n.r.	p value
ψ_G (Pct)	15	17	18	16	*
MA (μm)	29	29	30	36	n.s.
SF	0.07	0.07	0.08	0.07	n.s.
ψ_S (Pct)	0.3	0.4	0.5	1.0	**
EP (Pct)	10	10	9	11	n.s.
EC (cm^{-2})	20	19	17	17	*

All abbreviations as in Table III.
n.r. = not reported.
p values: * < 0.05; ** < 0.01; n.s. = not significant.

Fig. 5—Box plots of area fraction of graphite (ψ_G) in the matrix determined by image analysis of the optical micrographs in cross-section of the cast irons.

Considering the artifacts dating back to the second half of XIX century (box plots referring to cast iron samples from 1 to 15), the median value of the area fraction of manganese sulfides was the highest in CI_5 (ψ_S = 1.0 pct), and the lowest in CI_1 (ψ_S = 0.1 pct). Among the cast iron samples dating to the early XX century (box plots referring to samples from 16 to 24), the highest value was detected in CI_16 (ψ_S = 1.5 pct) and the lowest in CI_17 (ψ_S = 0.2 pct). Among the cast iron samples dating to the early XXI century (box plots referring to samples from 25 to 29), the highest value was detected in CI_26 (ψ_S = 1.0 pct) and the lowest in
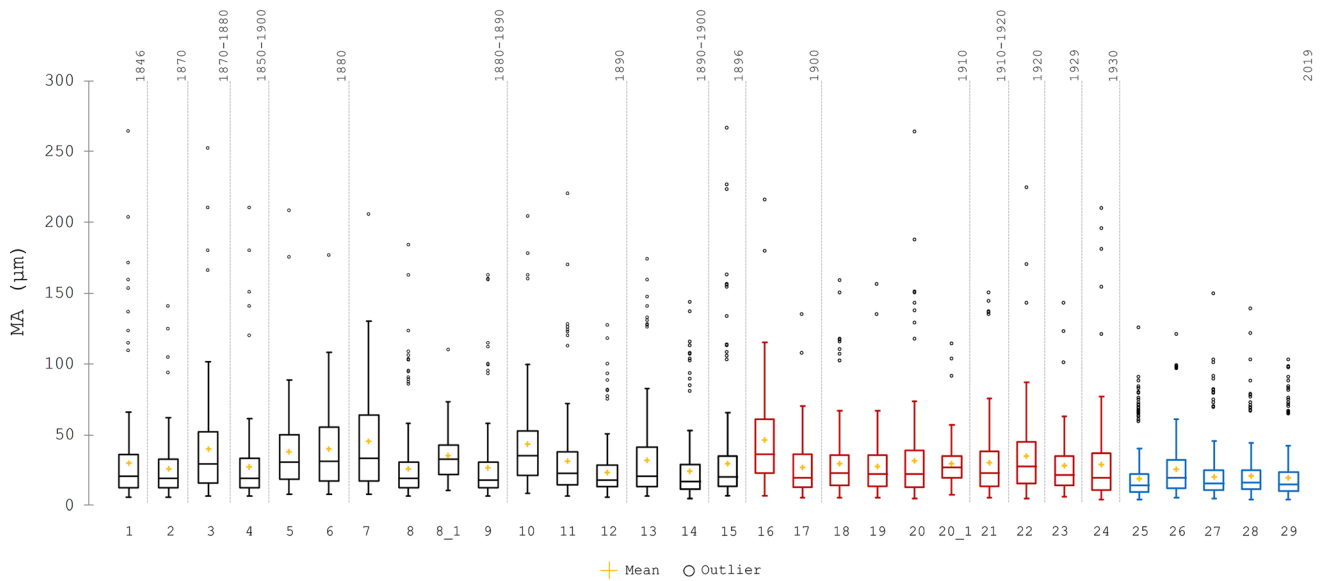
Fig. 6—Box plots of major axis of graphite lamellae (MA) determined by image analysis of the optical micrographs in cross-section of the cast irons.
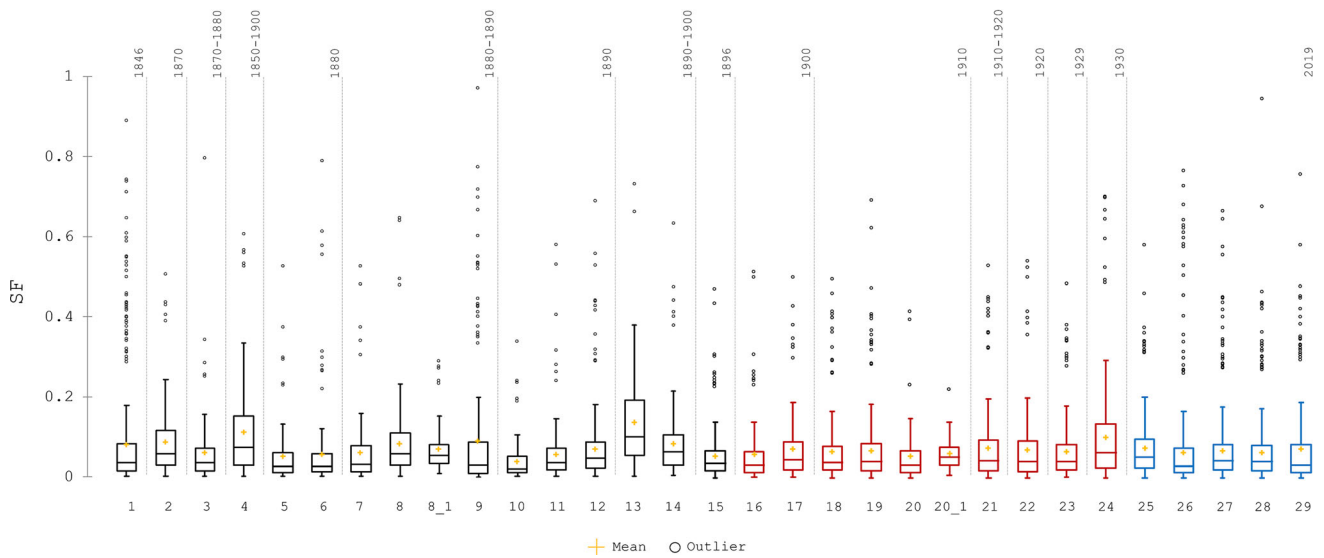

Fig. 7—Box plots of shape factor of graphite lamellae (SF) determined by image analysis of the optical micrographs in cross-section of the cast irons.

CI_29 (ψ_S = 0.4 pct). Considering all cast iron samples, the maximum and minimum values were those of CI_16 and CI_1. As supported by our chemical analyses, sulfur is mostly present in gray cast irons in the range from 0.02 to 0.15 pct in form of residual impurity from the foundry process.[33] The raw materials usually employed in the furnaces for melting and manufacturing cast irons are pig iron, cast iron, and/or steel scraps, fluxes (limestone as slag-forming elements), and coke. As already mentioned in Section II., during casting manganese binds to sulfur yielding favorable manganese sulfide inclusions. The highest values of ψ_S (corresponding to the highest values of sulfur detected by GDOES) in the artifacts CI_5, CI_16, and CI_22 could be due to the common practice of re-melting the obsolete street

furniture, associated with recycling of cast iron and/or steel scraps.[1,34,35] Nowadays, only a quarter of the Victorian street furniture in cast iron has been preserved: the remaining has been lost or replaced because of changes in artistic taste and/or improvements in lighting technology.[1]

Box plots of area fraction of steadite determined by image analysis of the optical micrographs in cross-section of the cast irons are shown in Figure 9. Considering the artifacts dating back to the second half of XIX century (box plots referring to cast iron samples from 1 to 15), the median value of the area fraction of steadite was the highest in CI_7 (EP = 15 pct), and the lowest in CI_4 (EP = 7 pct). Among the cast iron samples dating to the early XX century (box plots referring to samples
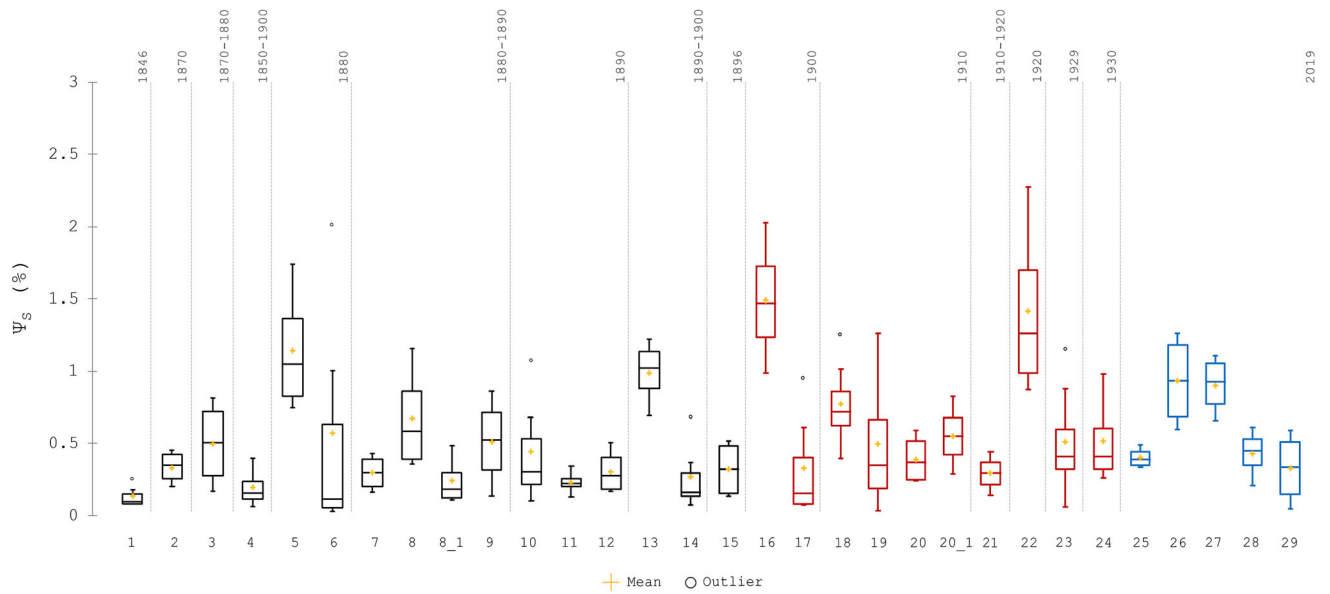
Fig. 8—Box plots of area fraction of manganese sulfides (ψ_S) determined by image analysis of the optical micrographs in cross-section of the cast irons.
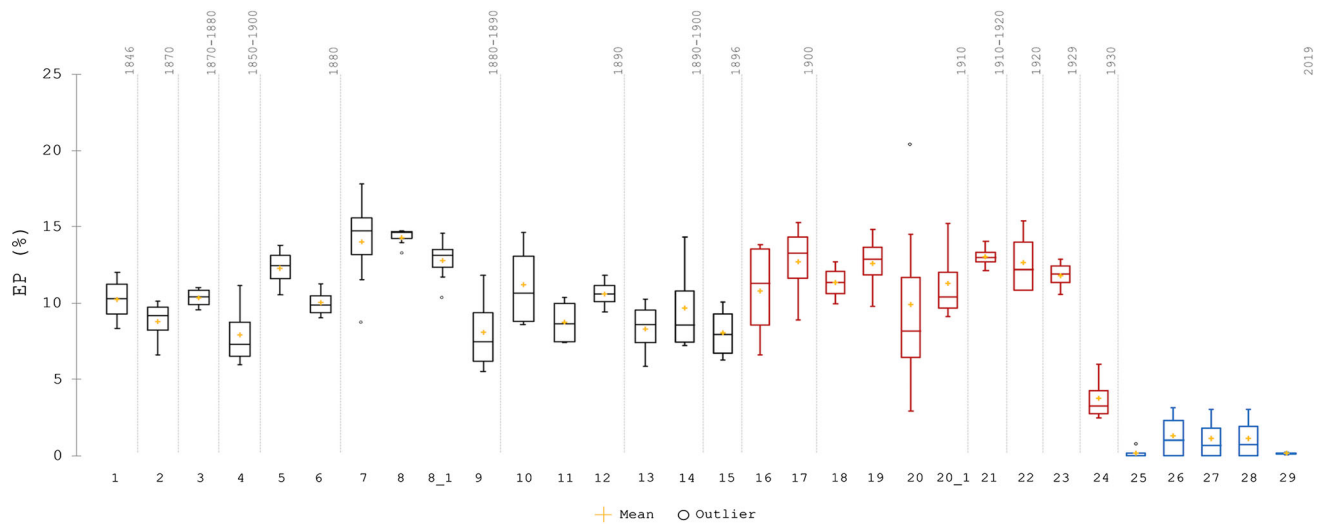

Fig. 9—Box plots of area fraction of steadite (EP) determined by image analysis of the optical micrographs in cross-section of the cast irons.

from 16 to 24), the highest value was detected in CI_17 (EP = 13 pct) and the lowest in CI_24 (EP = 3 pct). Among the cast iron samples dating to the early XXI century (box plots referring to samples from 25 to 29), the highest value was detected in CI_26 (EP = 1 pct) and the lowest in CI_29 (EP = 0.2 pct). Considering all cast iron samples, the maximum and minimum values were those of CI_7 and CI_29. As confirmed by our chemical analyses, steadite is found in gray cast irons with phosphorus content higher than 0.02 pct. High percentages of this element are usually accepted in castings and/or decorations for street furniture similar to those analyzed in this study: they require low solidification intervals and show an excellent castability, but they have low mechanical strength and toughness. Steadite, one of the last phases to solidify, hardens the

matrix, thus improving the wear resistance.[33] The lowest values of EP (corresponding to the lowest values of phosphorous detected by GDOES) in metalworks dating back to the early XXI century could be due to simpler geometries required for modern street furniture, for which a lower castability is allowed.[1]

Box plots of number of eutectic cells per area unit determined by image analysis of the optical micrographs in cross-section of the cast irons are shown in Figure 10. Considering the artifacts dating back to the second half of XIX century (box plots referring to cast iron samples from 1 to 15), the median value of the number of eutectic cells per area unit was the highest in CI_12 (EC = 31 cm^{-2}), and the lowest in CI_15 (EC = 7 cm^{-2}). Among the cast iron samples dating to the early XX century (box plots referring to samples from 16 to 24),

the highest value was detected in CI_17 (EC $= 24$ cm^{-2}) and the lowest in CI_16 (EC $= 9$ cm^{-2}). Among the cast iron samples dating to the early XXI century (box plots referring to samples from 25 to 29), the highest value was detected in CI_28 (EC $= 24$ cm^{-2}) and the lowest in CI_25 (EC $= 17$ cm^{-2}). Considering all cast iron samples, the maximum and minimum values were those of CI_12 and CI_15. It is generally accepted that the number of eutectic cells per area unit is an indication of the number of nuclei on which solidification has occurred.[36] The relevant event concerning cell structure is that it develops after the precipitation of austenite dendrites, thus cell growth superimposes on the dendritic structure.[36] Overheating and time of exposure to high temperature reduce the number of solidification nuclei (and consequentially EC), while inoculants as sulfur or iron-based silicates produce the opposite effect.[30] Finally, undercooling of the melt to lower temperatures (high degrees of undercooling) increases the number of solidification nuclei which are however of lower size.[37] In all the studied cast iron samples, the presence of lamellar graphite of Type A and B reveals low to intermediate degrees of undercooling, also supported by the low values of EC. The only exceptions are the cast iron samples CI_12 and CI_14, in which the presence of lamellar graphite of Type B + D was detected. These two samples underwent higher degrees of undercooling, as supported by the high EC values.

A summary of the median values of microstructural features determined by image analysis of the micrographs in cross-section of the cast iron parts is reported in Table V.

To discriminate the differences based on dating and nationality groups, the stepwise LDA was applied to all data (Tables II and III) as described in Section III. Among all functions calculated by the program, two functions were chosen as best discriminants among all data sets. Concerning the values in Table II, the plot of the first discrimination function (F1) against that of the second one (F2) for dating groups is shown in Figure 11. The LDA allowed to discriminate the cast irons with a validation of 82.76 pct, confirming the possibility to identify each artifact in relation to date. The high discrimination among cast irons is linked to F1, in which the microstructural features selected (p value < 0.01) by the forward stepwise progress for the discriminant plots are EP and MA (Figure 11).

For values of microstructural features shown in Table III, the LDA analysis was performed for nationality groups in the same conditions (Figure 12). The LDA model yielded 70.86 pct of validation for the cast irons and was able to discriminate all artifacts according to the nationality of the foundry of origin. The microstructural features selected by the forward stepwise for the discriminant plots were ψ_S and EC (Figure 12).

Concerning the classification based on dating, the results showed that the microstructural features depended on the year of manufacturing of the cast irons. The LDA multivariate analysis also enabled to discriminate our metalworks in relation to the nationality of the foundry of origin. The cast irons produced in United Kingdom and France and those of unreported origin were well discriminated, whereas the artifacts from Italy had mixed microstructural features, similar to
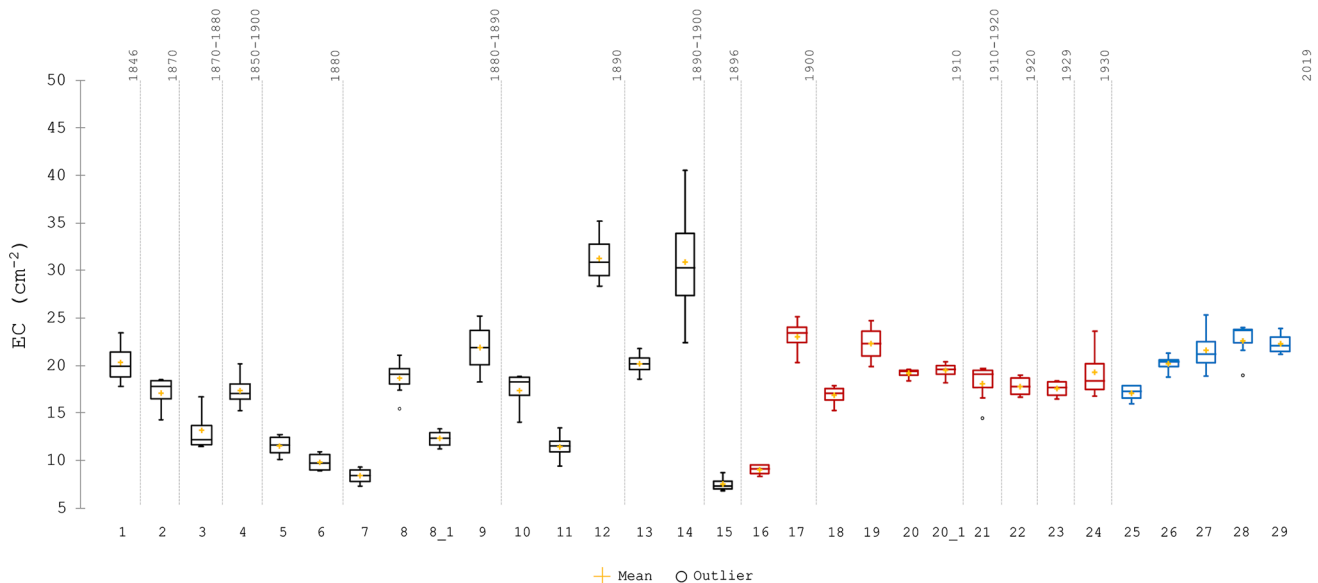

Fig. 10—Box plots of number of eutectic cells per area unit (EC) determined by image analysis of the optical micrographs in cross-section of the cast irons.

Table V. Summary of the Median Values of Microstructural Features Determined by Image Analysis of the Micrographs in Cross-Section of the Cast Iron (CI) Parts

CI part	ψ_G (Pct)	MA (μm)	SF	ψ_S (Pct)	EP (Pct)	EC (cm^{-2})
CI_1	22	21	0.04	0.1	10	20
CI_2	18	20	0.06	0.4	9	18
CI_3	19	30	0.04	0.5	10	12
CI_4	25	20	0.07	0.2	7	17
CI_5	10	31	0.03	1.0	12	11
CI_6	13	31	0.03	0.1	10	10
CI_7	13	33	0.03	0.3	15	8
CI_8	21	19	0.06	0.6	15	19
CI_8_1	15	32	0.05	0.2	13	12
CI_9	10	18	0.03	0.5	7	22
CI_10	13	35	0.02	0.3	11	18
CI_11	17	23	0.04	0.2	9	11
CI_12	18	18	0.05	0.3	11	31
CI_13	12	21	0.1	1.0	9	20
CI_14	20	18	0.06	0.2	9	30
CI_15	18	21	0.04	0.3	8	7
CI_16	15	37	0.03	1.5	11	9
CI_17	13	21	0.05	0.2	13	24
CI_18	15	24	0.04	0.7	11	17
CI_19	13	23	0.04	0.4	13	22
CI_20	20	23	0.03	0.4	8	19
CI_20_1	16	28	0.05	0.6	10	19
CI_21	17	24	0.04	0.3	13	19
CI_22	13	28	0.04	1.3	12	18
CI_23	13	23	0.04	0.4	12	18
CI_24	18	21	0.06	0.4	3	18
CI_25	18	15	0.05	0.4	0.2	17
CI_26	15	21	0.03	1.0	1	20
CI_27	17	17	0.04	1.0	1	21
CI_28	17	18	0.04	0.5	1	24
CI_29	11	16	0.03	0.4	0.2	22

All abbreviations as in Table III.
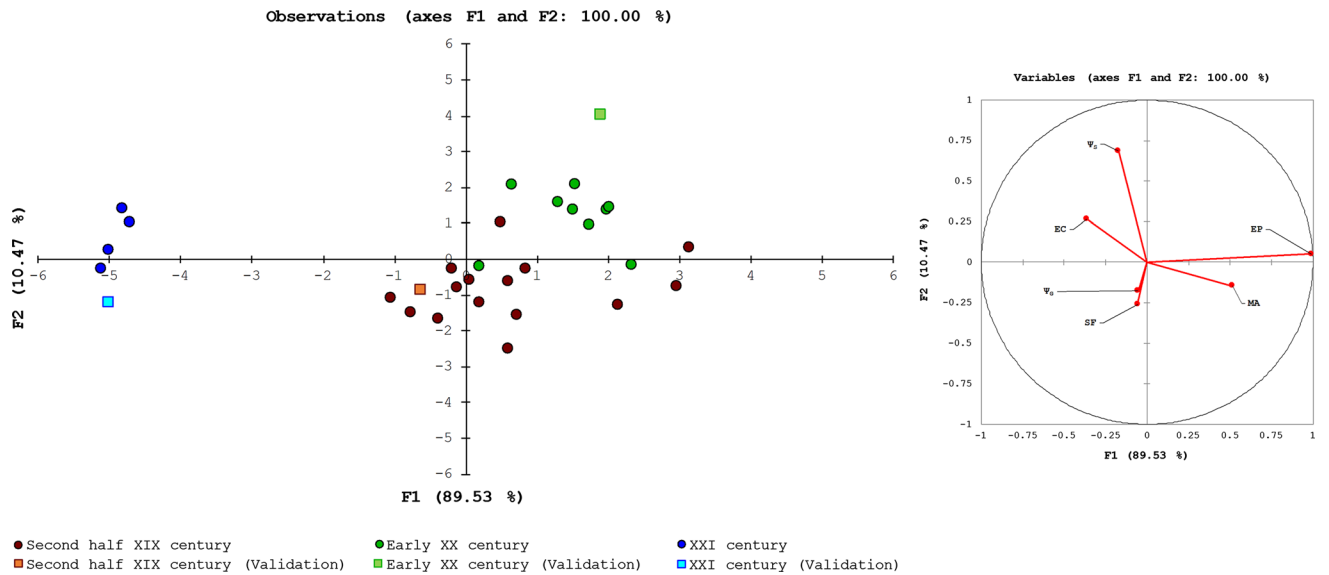
Fig. 11—Linear discriminant analysis (LDA) plots of microstructural features grouped according to dating of cast iron artifacts. Squares indicate the cross validation data.
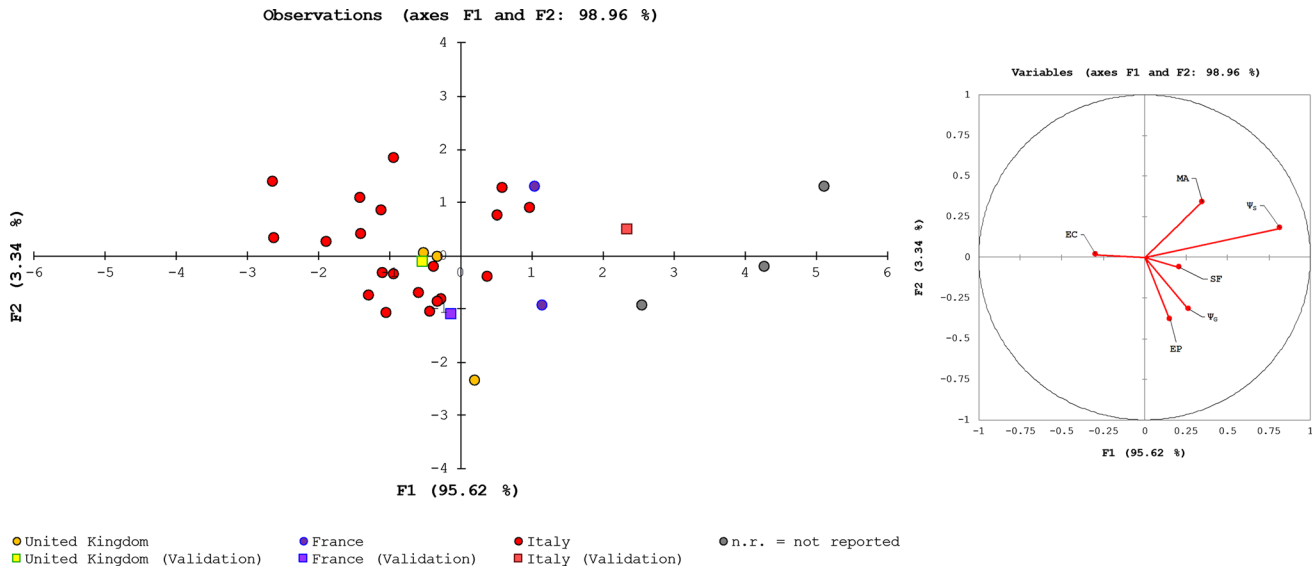
Fig. 12—Linear discriminant analysis (LDA) plots of microstructural features grouped according to nationality of the foundry of origin of the artifacts. Squares indicate the cross validation data.

those of the cast irons produced in the other two European countries. This result could be explained by the fact that United Kingdom and France pioneered the production of cast iron street furniture, while Italy duplicated foreign designs and imported foreign workers and materials. Only from the end of XIX century onwards, Italy developed an autochthonous cast iron production.[6]

V. CONCLUSIONS

Our study investigates the evolution of microstructure in relation with dating and nationality of the foundry of origin in twenty-four cast iron artifacts of street furniture produced between XIX and XX centuries. Among these artifacts, twenty-one came from foundries located in United Kingdom, France, and Italy, and three were of unreported origin. Although no data are available about the manufacturing techniques of the examined artifacts, the results showed that chemical composition of the alloys and form, distribution, and size of graphite in the studied microstructures were compatible with those of cast iron objects produced in the XIX and XX centuries. This is confirmed by the measurements of the area fraction of graphite (ψ_G) in the matrix, major axis (MA), and shape factor (SF) of graphite lamellae, and number of eutectic cells per area unit (EC). In some cases, the mean values of the area fraction of manganese sulfides (ψ_S) suggested re-melting of cast irons, associated with recycling of cast iron and/or steel scraps. Concerning the mean area fraction of steadite (EP), the high values found in the metalworks are in agreement with the excellent castability required to produce complex shape castings in the XIX and XX centuries. On the contrary, the low values of steadite found in contemporary artifacts could be due to the simpler geometries chosen for present day street furniture.

Finally, the LDA multivariate analysis allowed to detect a correlation between the microstructural features and the year of manufacturing and the nationality of the studied cast irons. Based on LDA data, the microstructural features useful as possible discriminants of these artifacts are the following in order of relevance: EP, MA, and ψ_S. Concerning the nationality, the LDA analysis enabled to discriminate cast irons produced in United Kingdom and France from those produced in Italy and also identify the penchant of Italy to duplicate designs from the other two European countries until the end of XIX century.

REFERENCES

1. R. Bassi and L. Bazzocchi: *So Light and Yet a Metal—The Art of Cast Iron in the 19th and 20th Centuries*, Manduria, Barbieri Selvaggi Editori, 2011, pp. 33–34.
2. A.C. de Ruggiero, L. Calzolari, C. Soffritti, A. Varone, and G.L. Garagnani: *Mater. Sci. Forum*, 2018, vol. 941, pp. 663–67.
3. C.R. Gagg and P.R. Lewis: *Eng. Fail. Anal.*, 2011, vol. 18, pp. 1963–80.
4. S. Godfraind, R. Pender, and B. Martin: *Metals—English Heritage*, Ashgate Publishing Ltd., Farnham, Practical Building Conservation, 2012.
5. P. Dobraszczyk: *Iron, Ornament and Architecture in Victorian Britain. Myth and Modernity, Excess and Enchantment*, Ashgate Publishing Ltd., Farnham, 2014.
6. C. Soffritti, L. Calzolari, A. Balbo, M. Chicca, R. Bassi Neri, A. Neri, L. Bazzocchi, and G.L. Garagnani: *Endeavour*, 2020, vol. 44, pp. 1–15.
7. C. Soffritti, L. Calzolari, A. Balbo, F. Zanotto, C. Monticelli, F. Ospitali, A. Fortini, and G.L. Garagnani: *Eur. Phys. J. Plus*, 2019, vol. 134, pp. 424–38.
8. C. Soffritti, L. Calzolari, A. Balbo, F. Zanotto, C. Monticelli, A. Fortini and G.L. Garagnani, *Metall. Ital.*: 2018, vol. 4, pp. 5–16.
9. J.R. Davis: *ASM Specialty Handbook*, Cast Irons, ASM International, Materials Park, OH, 1996.
10. R.F. Tylecote: *The early History of Metallurgy in Europe*, Longman Inc., New York, 1987.
11. N.C. Cox: *Ind. Archaeol. Rev.*, 1990, vol. 12, pp. 127–144.
12. K.H.J. Buschow, R. Cahn, M. Flemings, B. Ilschner, E. Kramer, S. Mahajan, and P. Veyssiere: *Encyclopedia of Materials: Science and Technology*, Pergamon Press Ltd., Oxford, 2001.
13. D.B. Wagner: *Iron and steel in ancient China*, BRILL, Leiden, 1996.
14. *J. Am. Foundrymen's Assoc.*, 1896, vol. 1.
15. D.M. Stefanescu: *Mat. Sci. Eng. A*, 2005, vols. 413–414, pp. 322–33.
16. E. Nechtelberger, H. Puhr, J.B. von Nesselrode and A. Nakayasu: *Cast iron with vermicular/compacted graphite—State of the art. Development, production, applications*, Proceedings of the 49th International Foundry Congress, CIATF, Chicago, 1982, Paper 1, pp. 1–39.
17. H.T. Angus: *Cast Iron. Physical and Engineering Properties*, Butterworth & Co. (Publishers) Ltd., London, 1976.
18. R. Gundlach, M. Meyer, and L. Winardi: *Int. J. Metalcast.*, 2015, vol. 9, pp. 69–82.
19. R.B. Gundlach: *AFS Trans.*, 2014, vol. 122, pp. 287–303.
20. H.R. Abbasi, M. Bazdar, and A. Halvaee: *Mat. Sci. Eng. A*, 2007, vol. 444, pp. 314–17.
21. I. Minkoff: *The physical metallurgy of cast iron*, John Wiley and Sons, Hoboken, 1983.
22. W.F. Smith: *Structure and Properties of Engineering Alloys*, RR. Donnelley and Sons Company, Chicago, 1981.
23. W.J. Tomlinson and G. Dennison: *Tribol. Int.*, 1989, vol. 22, pp. 259–64.
24. Standard EN ISO 945-1:2008 "Microstructure of cast irons—Part 1: Graphite classification by visual analysis".
25. A. Vaško: *Mater. Today Proc.*, 2016, vol. 3, pp. 1199–1204.
26. J. Grum and R. Šturm: *Acta Stereol.*, 1995, vol. 14 (12), pp. 91–96.
27. G.F. Vander Voort: *Metallography. Principles and Practice*, ASM International, Materials Park, OH, 2000.
28. J. Rys: *Stereology of Materials*, Fotobit Design, Cracow, 1995.
29. A.C. Rencher: *Methods of Multivariate Analysis*, 2nd ed., Wiley, Hoboken, 2002.
30. L. Collini, G. Nicoletto, and R. Konečná: *Mat. Sci. Eng. A-Struct.*, 2008, vol. 488, pp. 529–39.
31. M.M. Jabbari Behnam, P. Davami, and N. Varahram: *Mat. Sci. Eng. A.*, 2010, vol. 528, pp. 583–88.
32. Th. Willidal, W. Bauer, and P. Schumacher: *Mat. Sci. Eng. A*, 2005, vols. 413–414, pp. 578–82.
33. J.A. Pero-Sanz Elorz, D.F. González and L.F. Verdeja: *Physical Metallurgy of cast irons*, Springer, Cham, 2018.
34. D. Woodward: *Econ. Hist. Rev.*, 1985, vol. 38, pp. 175–91.
35. R. Fleming: *Past Present*, 2012, vol. 217, pp. 3–45.
36. J. Hemanth and K.V.S. Rao: *J. Mater. Eng. Perform.*, 1999, vol. 8, pp. 417–23.
37. J. Hemanth: *J. Mater. Eng. Perform.*, 2001, vol. 10, pp. 212–19.